Journal of Environmental Health Science and Engineering (2022) 20:101–112
https://doi.org/10.1007/s40201-021-00758-y

RESEARCH ARTICLE

Enhanced photocatalytic activity of Fe_2O_3@ZnO decorated CQD for inactivation of Escherichia coli under visible light irradiation

Motahare Harati[1] · Ahmad Jonidi Jafari[1,2] · Mahdi Farzadkia[1,2] · Roshanak Rezaei Kalantary[1,2]

Received: 31 August 2021 / Accepted: 30 October 2021 / Published online: 13 January 2022

Abstract

The present study, magnetically separable Fe_2O_3@ZnO/CQD nanocomposite was successfully prepared via hydrothermal process and characterized with SEM-EDX, XRD, FTIR, VSM and DRS analysis. The effect of operational parameters includes photocatalyst dosage, photocatalyst type, CQD content and *Escherichia coli (E. coli)* concentration were evaluated on the *E. coli* inactivation. The disinfecting ability of nanocomposite components was obtained as Fe_2O_3@ZnO/CQD> Fe_2O_3@ ZnO> ZnO> Fe_2O_3> CQD which shows a synergetic effect among different components. The highest *E. coli* inactivation rate (K_{max}=0.7606 min^{-1}) was obtained at photocatalyst dosage of 0.2 g/L and 15% CQD content. The MIC and MBC values value for *E. coli* were determined 0.1172 mg/mL and 0.4948 respectively that the results tests proved the antibacterial functions of the Fe_2O_3@ZnO/CQD. Nanocomposite showed the high reusability after 4 consecutive cycles, K_{max} decreased from 0.7606 min^{-1} to 0.6181 min^{-1}. Quenching experiments showed $^{\bullet}OH$ and h^+ are the main reactive oxygen species involved in the *E. coli* inactivation.

Keywords Photocatalytic inactivation · *Escherichia coli* · Fe_2O_3@ ZnO/CQD

Introduction

Drinking water quality has close relationship in people's health. It is estimated that 1.1 billion people suffer from the access to the safety water supplies worldwide. 2.2 million deaths are attributed to this issue, especially in children in developing countries [1–3]. Infectious diseases caused by waterborne pathogens not only make illness or death, but also have negative feedback on the medical expenses on economies and productivity losses [3]. One of the most common enteric pathogens is *Escherichia coli* (*E. coli*). The *E. coli* is a facultative anaerobic gram-negative strain, which is catalase positive and disrupts the intestinal tract of humans and other vertebrates; it is responsible for gastrointestinal diseases [4]. This specie is as an indicator to determine microbial quality of water, which has been probably polluted by fecal contamination [3, 5, 6]. To remove pathogen "particularly *E. coli*", there are many different methods such as advanced coagulation [3, 7], chlorination and other conventional oxidant [2, 3, 8, 9], membranes [10, 11], photocatalytic processes [12–15]. Physical operation for the removal of pathogens suffer from some disadvantage such as management and post treatment for produced residues, concentrating pathogens without inactivation, pathogen's regrowth, high energy consumption and need to large installations [3, 16]. Chlorination is commonly used for pathogen removal and disinfection process, especially *E. coli* in water treatment facilities. However, with respect to applicability and effectiveness of disinfection process, this process is not eco-friendly and some organism is resisted to the applied chemicals [11–13]. Semiconductor photocatalysis is a possible alternative for point-of-use water disinfection which introduced as the best and environmentally friendly approach in the inactivation of bacteria. Moreover, photocatalytic inactivation has shown a remarkable inactivation effect against many pathogens such as bacteria and fungi. Reactive oxygen species (ROS) are the main factors produced in the photocatalytic process which contribute in the bacteria inactivation mechanism. [17]. Recently, the nano-sized

✉ Roshanak Rezaei Kalantary
rezaei.r@iums.ac.ir

[1] Department of Environmental Health Engineering, School of Public Health, Iran University of Medical Sciences, Tehran, Iran

[2] Research Center for Environmental Health Technology, Iran University of Medical Sciences, Tehran, Iran

semiconductor materials with distinctive photo-induced electron-hole (e^-/h^+) pairs including ZnO,WS_2, ZnS, and TiO_2 have been extensively used in the photocatalytic processes for removal of pollutants [16, 18, 19]. Zinc oxide (ZnO) is the eco-friendly, low-cost, and highly biocompatible semiconductor that has been employed as the most potential photocatalyst for pollutants removal and pathogens inactivation [20–23].

The visible light photocatalytic activity of ZnO is restricted due crystal defect in the ZnO lattice and its wide gap band (3.3 eV) which cause the rapid recommendation of photogenerated e^-/h^+ pairs [24, 25]. Metal (such as Fe, Cu), and non-metal (such as N, P) elements are the promising alternative that can be replaced in the semiconductor lattice and retrieve crystal defect [18, 26]. Iron (Fe) is the most prevalent metal oxide that has been used for decreasing the semiconductor's gap band and improve photocatalytic activity [4, 27, 28]. Ferric oxide (Fe_2O_3) is a semiconductor with a hexagonal crystal structure (Fe atoms surrounded by six oxygen atoms) that generates e^-/h^+ pairs upon photoirradiation. Furthermore, Fe_2O_3 with Eg = 2.1 eV has been successfully used for improved the photocatalytic activity of different semiconductor such as Fe-loaded CeO_2 [29], Fe doped ZnO [30], Au/TiO_2-Fe_2O_3 [31, 32]. Li N et al. have reported Fe_2O_3 improved the photocatalytic activity of ZnO via increasing the surface area, expanding the spectral Response range, and reducing electron-hole pair recombination [33]. Besides, loss of the consumed photocatalysts during a recovery operation in addition to increasing costs is a major disadvantage that has adverse effects on the environment. Therefore, Magnetic separation is a promising method for gathering the used photocatalysts. Herein, the Fe_2O_3 magnetic feature facilitates the proper separation of nanoparticles and prevents secondary contamination [34].

Nowadays, researchers have been used carbon quantum dots (CQDs) in the synthesis of efficient photocatalysts. CQDs are the new nano-size materials in range of 2–10 nm in diameter [35]. The CQDs possess higher ability for charge transport in result of their high capability of transferring e^-/h^+ pairs and reservoir performances. Moreover, they have superior up-conversion photoluminescence, which can transmute UV to visible light, near UV, and visible light with shorter wavelengths. Hence, they can increase the light-utilized efficiency [36]. Recently, the researchers have been reporting the expanding studies of CQDs modified photocatalysts, such as Fe_3O_4/CQDs [37], N-doped CQDs, $ZnFe_2O_4$, and BiOBr [38], CQD/N-ZnO [39]. To the extent of our knowledge, with this photocatalyst, the photocatalytic investigation on the *E. coli* inactivation has not been reported yet. Thus, this work aims to assess the *E. coli* inactivation using the novel Fe_2O_3@ZnO/CQD nanocomposite under visible light irradiation considering the effect of different parameters include photocatalyst dosage, photocatalyst type, CQD content and *E. coli* concentration.

Experimental

Materials

E. coli (ATCC25922) was supplied from Pasteur Institute of Iran. Chemicals and culture medium were purchased from Merck Company. A Half McFarland standard solution and Mueller Hinton Broth (MHB) were purchased from Merck (Merck KGaA, Darmstadt, Germany). Ascorbic acid, ethylene glycol, Fe $(NO_3)_3{\cdot}9H_2O$ (98%), Zn $(NO_{3CQD})_2{\cdot}6H_2O$, HNO_3, NaCl, HCl, NaOH and ethanol (99.9%; Aldrich) were purchased from Merck, Germany. All chemicals were used in analytical grade without further purification.

Bacterial suspension preparation

Nutrient broth medium was used to grow of *E. coli* strain at 37 °C for 24 (in aerobic conditions). One loopful of the suspension was striped by a sterile inoculating loop onto Mac Conkey agar and extra incubated for 48 h at 37 °C [3]. The *E. coli* culture was prepared as following: first of all, a normal saline solution (9%) was prepared and transferred into an autoclave (15 psi, 121 °C and 1 h) to sterilize that. Then, the suspension with density of 10^5 CFU/mL *E. coli* bacteria in the normal saline solution was made by addition 4000 µL of bacterial culture in peptone broth ($1.5{\times}10^8$ CFU/mL), respectively, at the room temperature. The prepared aqueous solution had natural pH (7) to inhibit bacterial damaging on influence of the osmosis phenomenon.

Synthesis process of the photocatalyst

Preparation of CQD

The CQD was synthesized by a hydrothermal method according to reference [22]. Briefly, 1.6 g ascorbic acid and 15 ml glycol were transferred to 25 mL ultrapure water. The solution was well dispersed by ultrasonic machine for 60 min. The uniform solution was transported into a Teflon-lined stainless autoclave, and then heated for 70 min at 160 °C. Then, to remove the larger particles, the obtained residuals were centrifuged for 30 min at 10000 rpm.

Preparation of Fe_2O_3@ ZnO/CQD

Fe_2O_3@ ZnO/CQD was synthesized according to the Y Huang et al. procedure [22]. Briefly, 0.76 g of Zn $(NO_3)_2{\cdot}6H_2O$ and 1.45 g of Fe $(NO_3)_2{\cdot}9H_2O$ were dissolved in 20 mL of DI water. The solution was stirred completely

in order to obtain a homogeneous solution. The solution pH was adjusted 13 by addition the 2 M NaOH. The resulting dark brown slurry accompanied with CQDs aqueous solution in different amounts (5, 15 and 25 wt%) were poured into a 100 mL stainless-steel autoclave at 120 °C for 6 h and then, cooled to ambient temperature. Finally, the precipitations were washed several times by DI water and ethanol and then dried at 70 °C for 24 h.

Characterization procedures

Scanning electron microscopy (SEM) (accelerating voltage of 15.0 kV) was employed to characterize the Fe_2O_3@ZnO/CQD morphology. The structural property of the obtained powders was characterized by the X-ray diffraction (XRD) analysis using Cu Kα radiation. The functional groups present in the nanocomposite were determined by Fourier-transform infrared spectroscopy (FTIR) spectra by using KBr pellet technique in the range 450 to 4000 cm^{-1}. The Differential reflectance spectroscopy (DRS) analysis were carried out using a Hitachi U-3010 UV-visible (UV-vis) scanning spectrophotometer. The magnetic properties of the Fe_2O_3@ ZnO/CQD photocatalyst were measured by a VSM 9600–1 (LDJ), at room temperature with a peak field intensity of 15 kOe.

Photocatalytic inactivation of E. coli

The photocatalytic inactivation of *E. coli* was investigated in a photo-reactor consists of a glass container (100 mL) which equipped by LED lamp (UV-Visible range, λ_{max}=450 nm, 9 w, intensity= 20 mW/Cm^2, manufactured by Philips, Holland) as radiation source, 5 Cm above the solution. Before switching on LED lamp, *E. coli* solution was continuously mixed in the dark for 1 h in order to achieve adsorption-desorption equilibrium. Subsequently, the system was exposed to visible light for different time (90 min). The effect of different parameters includes CQD content (5, 15, and 25 wt%), photocatalyst dosage (0.05, 0.1, 0.2, and 0.4 g), and density of *E. coli* (10^3, 10^5, and 10^7) were evaluated on the *E. coli* inactivation. Samples were collected during the photocatalytic inactivation in the regular interval, serially diluted (10-fold) with saline solution and immediately spread onto the plate content Mueller Hinton Broth (MHB). Plates were incubated for 24 h at 37 ± 0.5 °C in order to determine the cell survival (in cfu/100 ml). The experimental controls include photolysis (*E. coli* and light radiation without nanocomposite) and dark (*E. coli* and nanocomposite without light radiation) were conducted similarly.

MIC and MBC experiments

MIC experiments were conducted by using a micro dilution procedure according to the method proposed by the Clinical Laboratory Standards Institute (CLSI) [40]. 2-fold serial dilution of the Fe_2O_3@ZnO/CQD was prepared in sterile MHB for a testing concentration range of 0.01–1.250 mg/mL. Next, 100 µL from each dilution was poured into the microliter plate and inoculated with 5 µL of standard (1.5×10^7 CFU/mL) bacterial suspension. The microliter plates were incubated at 37 °C for 24 h. The lowest concentration of the Fe_2O_3@ZnO/CQD which inhibited visible growth was considered as the MIC. MBC analysis was conducted by culturing 10 µL of supernatant in wells without visible growth on nutrient agar plates. The light board was used to count the colonies grown on agar medium and then compared with the negative control (merely medium, inoculum, no the Fe_2O_3@ZnO/CQD). The lowest concentration of the Fe_2O_3@ZnO/CQD killed 99.9% of the original inoculum was recorded as MBC. The positive control sample consisted of inoculated MHB without the photocatalyst, while uninoculated MHB was used as the negative control sample. Following incubation at 37 °C for 48 h, the colony-forming units per milliliter (CFU/mL) were then calculated.

Quenching test

To deeper insight the possible mechanism of photocatalytic reaction in the *E. coli* inactivation, the corresponding scavengers of tert-butanol (0.5 mmol L^{-1}), KI (0.5 mmol L^{-1}), and Cr (VI) (0.05 mmol L^{-1}) were used as hydroxyl radical ($^{\bullet}OH$), Superoxide Radical ($O_2^{\bullet-}$), and Positive hole (h^+) respectively.

Result and discussion

Characterization

SEM-EDX

Figure 1 (a, and b) shows the morphologies and elements distribution of the Fe_2O_3@ZnO/CQD composites using the SEM-EDX technique. Figure 1(a) shows the SEM micrograph of the Fe_2O_3@ZnO/CQD particle size and distribution. As shown, the powders are an aggregate of the Fe_2O_3@ZnO/CQD particles with a uniform diameter. The pattern of elements distribution in the Fe_2O_3@ZnO/CQD was determined by EDX analysis (Fig. 1(b)). EDX result indicates the presence of Zn (0.71%), Fe (15.47%), O (44.79%) and C (39.02%) in the nanocomposite. The intensity of the peaks in Fig. 1(b) refer to the weight percentage of atoms in the Fe_2O_3@ZnO/CQD and the results show a very scarce presence of iron. Also, presence of atoms of C in high percent showed that the CQD well placed into the photocatalist particles.

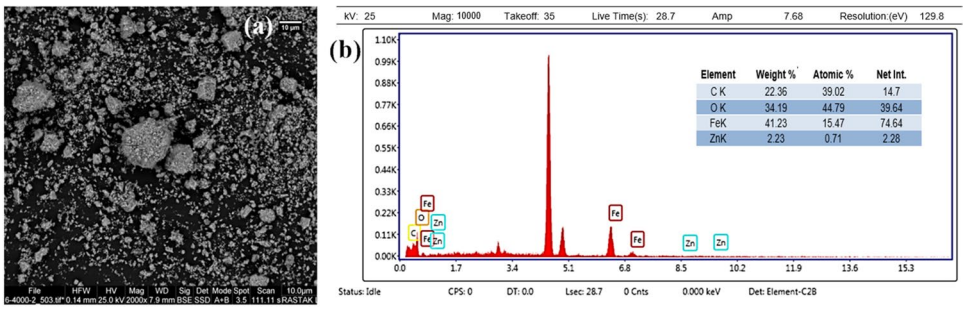

Fig. 1 The SEM-EDX image of (**a**) and (**b**) Fe_2O_3@ZnO/CQD

FTIR

The FTIR spectra for Fe_2O_3@ZnO/CQD composite are shown in Fig. 2 (a). The FTIR spectrum appears broad peak at 3413.80 cm^{-1} because of stretching vibration of O–H bond in free water. The peak at 1627.87 cm^{-1} is at ascribed to O–H bending vibration of adsorbed water. The peak at 2910 cm^{-1} is corresponded to symmetric stretching vibrations for CH_2 group [41]. The peak at 199.64 cm^{-1} arising from C–H scissoring vibration. It shows broad peak below 800 cm^{-1}, which attribute to the Ti–O bond stretching. The FTIR band at 567.26 cm^{-1} related to the magnetite form of iron oxide (Fe–O) [27]. The band of 817.23 cm^{-1} was known as the stretching mode of C-C. Besides these, the sharp peak at 1383.13 cm^{-1} relates to symmetric vibrations of COO− [38]. The observed peak at 479.48 cm^{-1} has corresponded to the metal-oxygen (M-O) stretching mode (Zn-O and Fe-O) [42, 43].

XRD

Figure 2 (b) shows the XRD patterns of the Fe_2O_3, Fe_2O_3@ZnO and Fe_2O_3@ZnO/CQD particles. The samples show the nine distinctive Fe_2O_3 peaks at 16.27 (111), 27.2 (211), 29.77 (220), 36.34 (311), 45.06 (400), 57.40 (442), 36.95 (511), 67.51 (440), and 83.95 (622), confirming that pore Fe_2O_3 is cubic spinel structure [42]. No more peaks are assigned to the crystalline form in Fe_2O_3@ZnO and Fe_2O_3@ZnO/CQD Fig. 2 (b).

DRS

The optical properties of the ZnO NP, CQD, and Fe_2O_3@ZnO/CQD was investigated using UV–Vis spectrophotometry. As illustrated in Fig. 2 (c), the ZnO NP plot exhibits the high absorption at UV band (<400 nm). Also, the CQD has

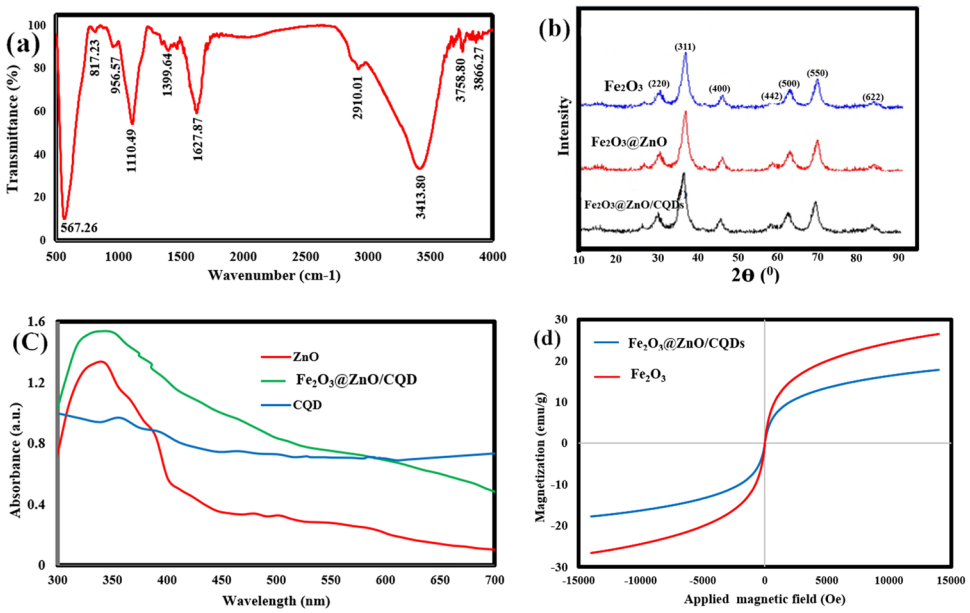

Fig. 2 **a** FTIR spectra and (**b**) XRD patterns of Fe_2O_3@ZnO/CQD, (**c**) UV-vis diffuse reflectance spectra (DRS), and (**d**) VSM image of the Fe_2O_3@ZnO/CQD

fundamental adsorption at broad band (300–700 nm). The Fe_2O_3@ZnO/CQD plot shows absorption at higher wavelength. The CQD and Fe co-doping increase the absorption wavelength of ZnO and shifted it to the visible region (longer wavelength). This causes the increasing photocatalytic activity of the Fe_2O_3@ZnO/CQD under visible light irradiation. In a similar study, Yu Huang et al. and Lu Li et al. have reported adding NCDs lead to more absorption of both UV and visible light by nanocomposite [44, 45].

The band gap energy was calculated using Kubelka-Munk principles as shown in the Eq. (2) [46]:

$$E_{g=}\frac{1{,}240}{\lambda} \quad (1)$$

The band gap energy for un-doped ZnO and Fe_2O_3@ZnO/CQD were 3.39 and 2.7 eV, respectively. All these samples indicated a decrease in band gap energy due to surface modification of ZnO.

VSM

Figure 2 (d) shows the magnetic hysteresis loops of the Fe_2O_3 and Fe_2O_3@ZnO/CQD powders. As seen in Fig. 2 (d), the magnetization values (Ms) of Fe_2O_3 and Fe_2O_3@ZnO/CQD were 26.5 and 18.2 emu/g respectively, indicating the strong magnetization. As seen, the Ms. of Fe_2O_3 was 26.5 emu/g which after decorating with ZnO/CQD reduced to 18.2. That show agglomeration ZnO and CQD could reduce magnetization power of main photocatalyst. Fe_2O_3@ZnO/CQD is suitable for magnetically separation by a magnetic field and separation of the photocatalyst from the aqueous solution. The recycled the Fe_2O_3@ZnO/CQD could be used to treat further solutions and thus reduced the cost of materials. Ahmadian-Fard-Fini et al. have been resulted that magnetic nanoparticles are covered by CQDs and as a result higher magnetic field is needed for changing in magnetic domains of the nanoparticles [47]. There are other studies that demonstrated effect of covering CQDs onto the photocatalysts [48, 49].

Photocatalytic inactivation efficiency

The process performance at different systems

The inactivation performance of different nanocomposite components (Fe_2O_3, ZnO, CQD, Fe_2O_3@ZnO and Fe_2O_3@ZnO/CQD) were evaluated in *E. coli* inactivation rate (Fig. 3). As can be seen, for the CQD, inactivation efficiency had depletion K_{max}= 0.00253 min^{-1}. It cleared that the CQD appeared very low efficiency for the *E. coli* removal because no ability seems to surface sorption or chemical oxidation for the CQD, so it could be because of light radiating [50].

In dark situation, Fe_2O_3 and ZnO had a little inactivation rate. The residuals were K_{max}= 0.0181 min^{-1} and K_{max}= 0.0312 min^{-1} for Fe_2O_3 and ZnO, respectively. Inactivation rate was to be more in light situation, where it was inactivation rate reached to K_{max}= 0.0463 min^{-1} and K_{max}= 0.1632 min^{-1} for Fe_2O_3 and ZnO, respectively. These phenomena showed when Fe_2O_3 and ZnO expose to the light in addition of adsorption mechanisms in in dark, little production of active radicals could be effective on the *E. coli* inactivation [51]. In the Fe_2O_3@ZnO and Fe_2O_3@ZnO/CQD systems, log count of *E. coli* reduced down to near zero in 30 min and 15 min, respectively. In those systems, production of $^{\bullet}OH$ radicals led to inactivation of *E. coli* under visible light (Eq. 1–11) [52]. Also, inactivation at short time in the Fe_2O_3@ZnO/CQD system showed being sufficient of supporting CQD on the Fe_2O_3@ZnO. Omran Moradlou et al. reported similar result for the CQD [12]. In dark situation, also, the Fe_2O_3@ZnO and Fe_2O_3@ZnO/CQD systems showed the acceptable inactivation for *E. coli* in 60 min. It may be because of the antibacterial characterization of those particles. Also, ZnO has antibacterial inherent properties [52].

$$Fe_2O_3@ZnO/CQD + h\upsilon_{(\lambda\geq 420\ nm)} \rightarrow e_{CB}^{-}\ (CQD) + h_{VB}^{+}\left(Fe_2O_3@ZnO\right) \quad (1)$$

$$h_{VB}^{+}\left(Fe_2O_3@ZnO\right) + OH^{-} \rightarrow OH^{\bullet} \quad (2)$$

$$h_{VB}^{+}\left(Fe_2O_3@ZnO\right) + H_2O \rightarrow OH^{\bullet} + H^{+} \quad (3)$$

$$e_{CB}^{-}\ (CQD) + O_2 \rightarrow O_2^{\bullet -} \quad (4)$$

$$2O_2^{\bullet -} + 2H^{+} \rightarrow H_2O_2 + O_2 \quad (5)$$

$$Fe^{+2} + O_2 \rightarrow Fe^{+3} + O_2^{\bullet -} \quad (6)$$

$$Fe^{+3} + e_{CB}^{-}\ (CQD) \rightarrow Fe^{+2} \quad (7)$$

$$Fe^{+2} + O_2^{\bullet -} + 2H^{+} \rightarrow Fe^{+3} + H_2O_2 \quad (8)$$

$$O_2^{\bullet -} + 2H^{+} \rightarrow O_2 + H_2O_2 \quad (9)$$

$$H_2O_2 + e_{CB}^{-}\ (CQD) \rightarrow OH^{\bullet} + OH^{-} \quad (10)$$

$$Fe^{+3} + H_2O + h\upsilon_{(\lambda\geq 420\ nm)} \rightarrow Fe^{+2} + OH^{\bullet} + H^{+} \quad (11)$$

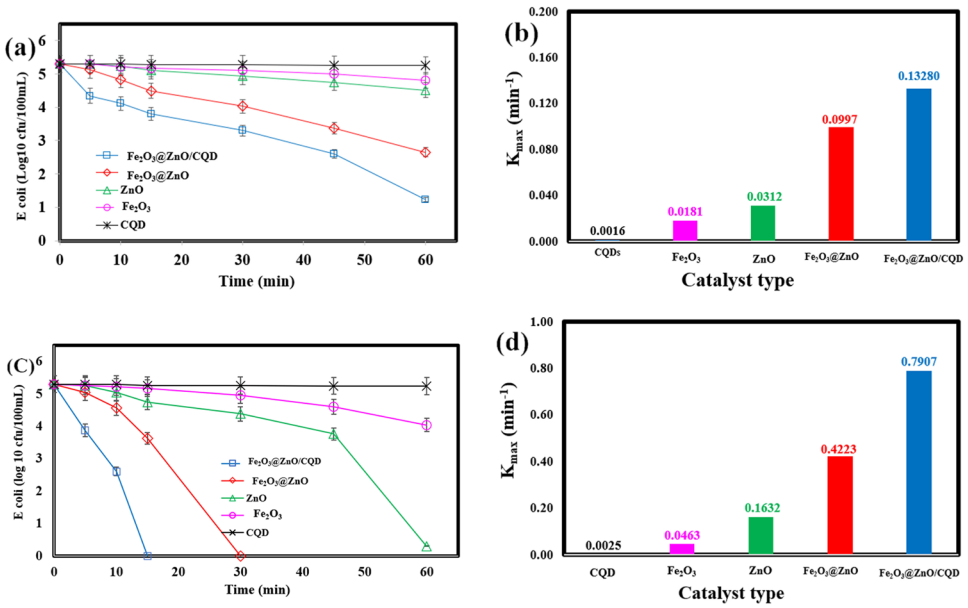

Fig. 3 **a** effect of catalyst type on *E. coli* inactivation in dark and (**b**) K_{max} of *E. coli* inactivation, (**c**) effect of catalyst type on *E. coli* inactivation in light and (**d**) K_{max} of *E. coli* inactivation (pH= 7; $[Catalyst]_0$= 0.2 g/100 mL; VL intensity= 90 mw/cm^2; $[E.\ coli]_0$= 10^5).

Effect of the CQD content

The photocatalytic *E. coli* inactivation was evaluated in the existence of different CQD content (%5, %15 and %25) (Fig. 4). *E. coli* inactivation rate was obtained for %5 (K_{max}= 0.1145 min^{-1}), (K_{max}= 0.2475 min^{-1}), %15 (K_{max}= 0.2477 min^{-1}), (K_{max}=0.7605 min^{-1}), and %25 (K_{max}= 0.0145 min^{-1}), (K_{max}= 0.05430 min^{-1}) CQD content, in dark and light respectively, which results showed that %15 CQD content has the highest *E. coli* inactivation rate in both dark and light conditions. The low inactivation rate in the 25% CQD content is due to occupying the photocatalyst pores by the CQD which eventually has limited the inactivation of *E. coli* bacteria [51].

CQD play role as a conduction center for exited electors while in high concentration scattering phenomenon inhabits receiving light the Fe_2O_3@ZnO photocatalyst. Accumulation of the CQD with nano sizes onto the dispersed the visible light radiated [27, 47]. On the other hand, the high CQD content ding hinders the interaction between Fe cations and *E. coli*. Because Fe^{3+} induce the change in the functional groups of proteins and lipopolysaccharides in the outer membranes of bacteria. Moreover, the diffusion of ferric ions inside the bacteria generates the ROSs which facilitates the bacteria inactivation [53]. Therefore, proper content of CQD via increase the photocatalytic activity causes more ROSs generation which contributes to the bacteria inactivation. CQD can improve the photocatalytic activity of the ZnO under visible light by

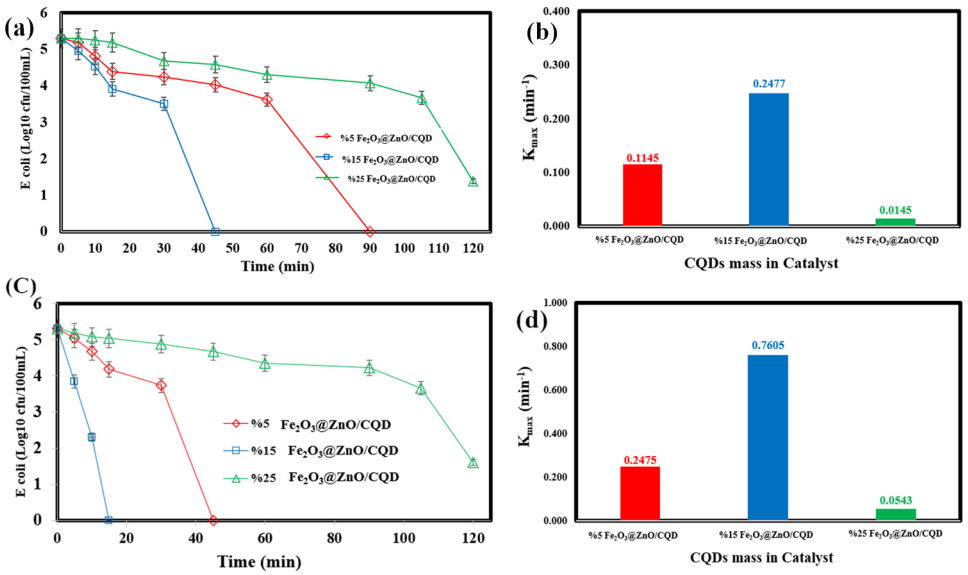

Fig. 4 **a** Effect of the CQD mass in the composition of nanocomposite in dark and (**b**) K_{max} of *E. coli* inactivation, (**c**) Effect of the CQD mass in the composition of nanocomposite in light and (**d**) K_{max} of *E. coli* inactivation (pH= 7; $[Catalyst]_0$= 0.2 g/100 mL; VL intensity= 90 mw/cm^2; $[E.\ coli]_0$= 10^5)

decreasing the e^-/h^+ pairs (migrate the e^- from ZnO to CQD) and shifting the catalytic feature of ZnO from the infrared spectral regions to the visible area (Eq. 12–21) [54]. Kuang W et al. have reported that the outer membranes of bacteria were changed to blur in the presence of CQD-ZnO. Also, CQD and ZnO induce the slight separation and disappear of outside bacteria membranes respectively [55].

$$Fe_2O_3@ZnO/CQD + h\upsilon_{(\lambda\geq 420\ nm)} \rightarrow e_{CB}^{-}\ (CQD) + h_{VB}^{+}\left(Fe_2O_3@ZnO\right) \quad (12)$$

$$e_{CB}^{-}\ (CQD) + O_2 \rightarrow O_2^{\bullet -} \quad (13)$$

$$h_{VB}^{+}\left(Fe_2O_3@ZnO\right) + OH^{-} \rightarrow OH^{\bullet} \quad (14)$$

$$O_2^{\bullet -} + H_2O \rightarrow HO_2^{\bullet} + OH^{-} \quad (15)$$

$$HO_2^{\bullet} + H_2O \rightarrow H_2O_2 + OH^{\bullet} \quad (16)$$

$$O_2^{\bullet -} + 2H^{+} \rightarrow H_2O_2 + OH^{\bullet} \quad (17)$$

$$Fe^{+3} + e_{CB}^{-}\ (CQD) \rightarrow Fe^{+2} \quad (18)$$

$$Fe^{+2} + H_2O_2 \rightarrow Fe^{+3} + OH^{-} + OH^{\bullet} \quad (19)$$

$$Fe^{+3} + OH^{-} + h\upsilon \rightarrow Fe^{+2} + OH^{\bullet} \quad (20)$$

$$2OH^{\bullet} \rightarrow \text{Destruction of bacteria cell wall} \quad (21)$$

Effect of the photocatalyst dosage

Fig. 5 shows the effects of different dosage of Fe_2O_3@ZnO/CQD (0.05, 0.1, 0.2, and 0.4 mg/100 mL) on the *E. coli* inactivation. As shown, in the dark situation, with increased photocatalyst dosage, *E. coli* inactivation was increased. It can be due to increase in sorption sites onto the nanocomposite. In the light situation, increase in dosage from 0.05 mg/100 mL up to 0.2 mg/100 mL increased inactivation of *E. coli*. At the dosage of 0.2 and 0.4 mg/100 mL, the K_{max} of *E. coli* reached 0.7606 min^{-1} and 0.2511 min^{-1} during 30 min and 45 min in light and K_{max}=0.1867 min^{-1} and K_{max}=0.2998 min^{-1} during 60 min and 45 min in dark respectively. This delay contributed to turbidity of particles in 0.4 mg/100 mL, which reduced irradiation intensity [1]. It is expected that with increase in photocatalyst mass while the other parameters are constant inactivation efficiency increase because of abundance of active sites where trapped visible light [56]. Masoud Moradi et al. have observed similar result [27]. The release of ferrous ions will be increased in high amount of catalyst dosage which led to increasing of Kmax in both dark and light conditions. On the other hand, high surface area facilitates the adsorption of more water molecules, consequently, a high amount of ROS will be generated due to the reaction between absorbed water molecules and positive holes (h+) of catalyst [27]. They demonstrated that the suspended photocatalyst in high value can make turbidity, and reduce light exposing [3, 27].

Effect of E. coli density

It is demonstrated bacterial death and growth occur in a logarithmic fashion [3, 27]. Therefore, density of bacteria can be an effective parameter to short inactivation time.

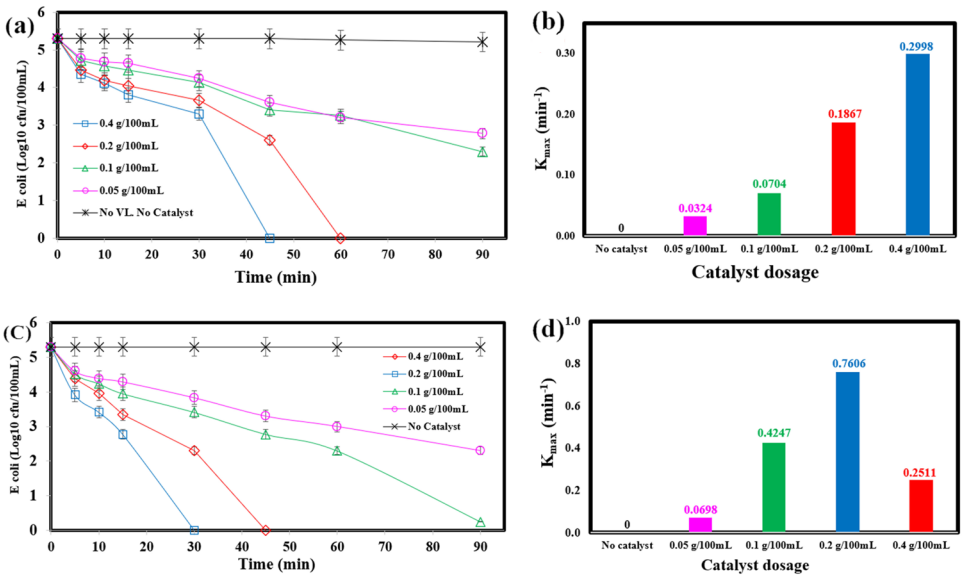

Fig. 5 **a** effect of catalyst dosages on *E. coli* inactivation in dark and (**b**) K_{max} of *E. coli* inactivation, (**c**) effect of catalyst dosages on *E. coli* inactivation in light and (**d**) K_{max} of *E. coli* inactivation (pH= 7; VL intensity= 90 mw/cm^2; [*E. coli*]$_0$= 10^5).

The *E. coli* bacteria in three different densities (10^3, 10^5 and 10^7 cfu/100 mL) were injected in the experimental solution (Fig. 6 a & b). As expected, in density of 10^3 (K_{max}= 0.9435 min^{-1}) and 10^5 cfu/100 mL (K_{max}= 0.7617 min^{-1}), *E. coli* was completely inactivated in less than 15 min. While, 60 min was required for complete inactivation of *E. coli* in density of 10^7 cfu/100 mL (K_{max}= 0.2294 min^{-1}). Because when ROS production is constant, the more time is needed for inactivation at high density of bacteria. Previous studies e.g. Sidali Kourdali et al., have been reported similar result [57]. On the other hand, high-loading bacteria occupy the active site of the photocatalysts and led to diminishing the photocatalyst performance However, biologists declare that increase of bacteria mass enhances their resistance against environmental treats and dangers. [3, 57, 58].

Quenching test

Fig. 6 c & d indicated the effect of different scavengers, tert-butanol > KI > Cr (VI), on the *E. coli* inactivation. As shown, when scavengers were added, the K_{max} was obtained in various amounts (tert-butanol: K_{max}= 0.0171 min^{-1}, KI: K_{max}= 0.1055 min^{-1}, Cr (VI): K_{max}= 0.4477 min^{-1}). tert-butanol have a lowest K_{max} (0.0171 min^{-1}) that $^{\bullet}OH$ played a significant specie in the inactivation E. coli. The results indicated that the inactivation rate constant decreased as KI (h^+ and $^{\bullet}OH$ scavenger) was added. The h^+ could be either penetrated to the *E. coli*, causing its inactivation, or was adsorbed by water molecules which generated $^{\bullet}OH$ [27]. When KI was added we observed less effective compared to tert-butanol indicating the moderate effect of h^+/$^{\bullet}OH$s in the inactivation process [27]. Yanning Qu et al. also have reported that on photodegradation removal of ciprofloxacin by ZnO/N,S-CQDs hybrid photocatalyst $^{\bullet}OH$ and $O_2^{\bullet-}$ play a crucial role [23]. As shown, addition of Cr (VI), had a far less effect on the E. coli inactivation, indicating less efficacy on $O_2^{\bullet-}$ in the system (Eq. 25–27) [27].

$$Cr_2O_7^{-2} + 14H^+ + 6e_{CB}^- \rightarrow 2Cr^{3+} + 7H_2O \quad (25)$$

$$HCrO_4^- + 7H^+ + 3e_{CB}^- \rightarrow Cr^{3+} + 4H_2O \quad (26)$$

$$3O_2^{\bullet-} + Cr^{6+} \rightarrow Cr^{3+} + O_2 \quad (27)$$

The MIC and MBC tests

Table 1 represent the MIC and MBC average values for E. coli treated using Fe_2O_3@ZnO/CQD. The MIC value for *E. coli* was determined 0.1172 mg/mL (Table 1). The MBC value was found to be 0.4948 mg/mL (Table 1). According to results in Table 1 related to the MIC or MBC values, it derived that the Fe_2O_3@ZnO/CQD photocatalyst has

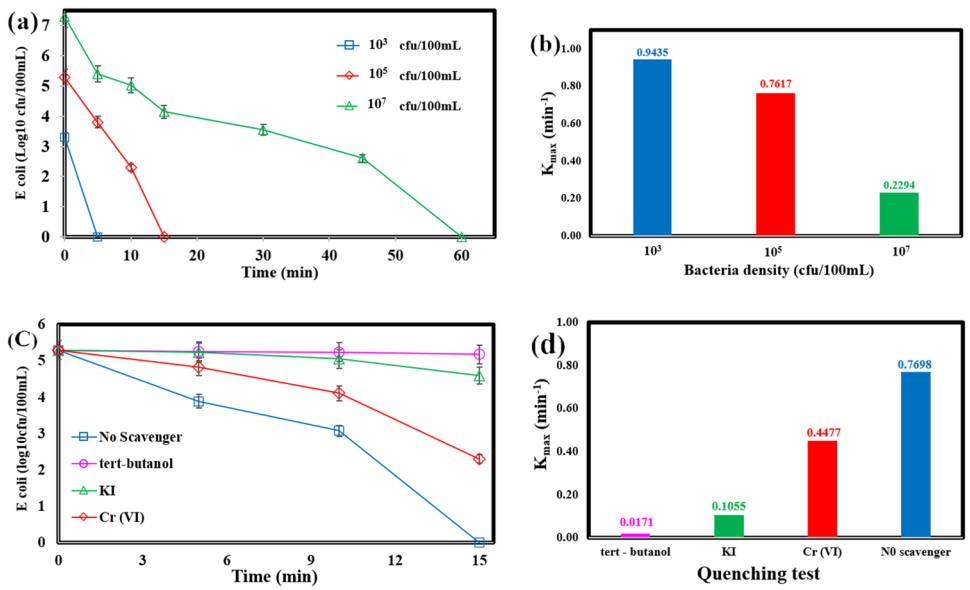

Fig. 6 **a** effect of bacteria density on the inactivation process and (**b**) K_{max} of *E. coli* inactivation, (**c**) effect of different scavengers on the inactivation process and (**d**) K_{max} of *E. coli* inactivation (pH= 7; $[Catalyst]_0$= 0.2 g/100 mL; VL intensity= 90 mw/cm^2; $[E. coli]_0$= 10^5).

Table 1 The MIC and MBC of the Fe_2O_3@ ZnO/CQD photocatalyst for *E. coli*

Sample	MIC (mg/mL)	MBC (mg/mL)
E. coli	0.1172	0.4948

antibacterial effect, and can be used as effective antibacterial matter. The researchers have reported similar antibacterial effects for the ZnO based photocatalyst [59, 60]. As well known, the ZnO has been conventionally used for antimicrobial purposes [59]. The potential for ZnO refers to entry the Fe_2O_3@ ZnO/CQD photocatalyst into the *E. coli* and to damage its cell wall, and finally to inactive *E. coli* bacteria [60]. According to MIC or MBC values (Tables 1), it is clear that Fe_2O_3@ ZnO/CQD has antibacterial effects and can be used as antibacterial agent. Previous studies have been shown that these antibacterial agents cause bacterial cell membrane damage, spatial deformation, degradation of bacterial [59, 60]. The control experiment showed that without a photocatalyst, the E. coli hardly decomposed during photolysis over a period of 60 to 90 min. However, illustrates a significant decrease in the height of the amount of the E. coli concentration during the photodegradation process. This character refers to end CQD in Fe_2O_3@ZnO/CQD structure which interact with negative charge of membrane or microorganism cytoplasm, causing bacterial cell wall damage and finally, inactivation of bacteria [60].

Photocatalyst reusability

The reusability of the photocatalysts is one of the main concerns in the environmental purification the technologies [61]. To investigate the reusability, the synthesized the Fe_2O_3@ZnO/CQD photocatalyst was separated magnetically from the reaction solution and washed by ethanol followed by water washing, and in consequence reused in 4 cycles after each 90 min. As seen in Fig. 7, the inactivation efficiency only revealed partial reduction after 4 cycles in the *E. coli* inactivation (K_{max}=0.1426 min^{-1}. These results demonstrated that our synthesized composite is a promising photocatalyst for purification of wastewater for inactivation *E. coli*.

Conclusion

The Fe_2O_3@ZnO/CQD was successfully prepared with a magnetic core by a hydrothermal method. The structure and optical features of the photocatalysts were characterized by SEM, FTIR, XRD, VSM, and DRS. The highly dispersed CQD on the surface of Fe_2O_3@ZnO considerably improved photocatalytic activity for inactivation of *E. coli* under visible light radiation. The CQD content up to 15% had positive effect in both dark (K_{max}=0.1332 min^{-1}) and light (K_{max}=0.513 min^{-1}) conditions. While 25% CQD content had decreased in dark (K_{max}= 0.2332 min^{-1}) and light (K_{max}=0.7062 min^{-1}) respectively. MICs and MBCs of the antimicrobial agents conducted in the present study were specified using the micro dilution test method. The MIC (0.1172 mg/mL) and MBC (0.4948 mg/mL) analysis cleared that the produced photocatalyst had antibacterial effect on the *E. coli*. The inactivation rate (K_{max}=0.7606 min^{-1}) achieved to optimum at 0.2 g/L of the photocatalyst, and then the K_{max} reduced. Increased in density of *E. coli* reduced the inactivation *E. coli*. Totally, the effect of scavengers was obtained as tert-butanol > KI > Cr (VI), which indicates a greater role of Cr (VI) in the inactivation of *E. coli*. KI slightly low effective compared to tert-butanol (h+ / $^{\bullet}$OHs scavenger) indicating the moderate effect in the inactivation process. The results indicated that in Fe_2O_3@ZnO/CQD by decreasing the gap band (ZnO), increased photocatalytic activity in the production of $^{\bullet}$OH. The quenching test suggested the $^{\bullet}$OH and h^+ radicals play a crucial role in the *E. coli* inactivation. It can be concluded the Fe_2O_3@ZnO/CQD photocatalyst can be used as an efficient magnetic base photocatalyst for E. coli inactivation in aqueous solutions. Finally, reusability experiment of the Fe_2O_3@ZnO/CQD photocatalyst showed that is a reusable photocatalyst and can be used for many times.

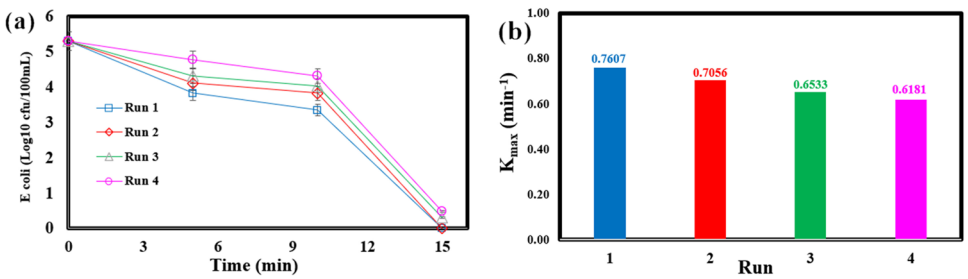

Fig. 7 **a** Reusability of the Fe_2O_3@ZnO/CQD and (**b**) K_{max} of *E. coli* inactivation (pH= 7; $[Catalyst]_0$= 0.2 g/100 mL; VL intensity= 90 mw/cm^2; $[E. coli]_0$= 10^5)

Acknowledgements The authors thankfully acknowledge the financial support given by the Iran University of Medical Sciences [grant No. 97-01-27-33424]. (Ethics Code: IR.IUMS.REC.1397.305).

Conflict of interest The authors of this article declare that they have no conflict of interests.

References

1. Taghavi K, Naghipour D, Mohagheghian A, Moslemzadeh M. Photochemical degradation of 2,4-dichlorophenol in aqueous solutions by Fe2+/ Peroxydisulfate/ UV process. Int J Eng. 2017;30:15–22 https://doi.org/10.5829/idosi.ije.2017.30.01a.03.
2. Jafari AJ, Moslemzadeh M. Investigation of phosphorus removal using steel slag from aqueous solutions : a systematic review study. Int J Environ Anal Chem. 2020;00:1–13 https://doi.org/10.1080/03067319.2020.1726900.
3. Jafari AJ, Mahrooghi M, Moslemzadeh M. Removal of Escherichia coli from synthetic turbid water using titanium tetrachloride and zirconium tetrachloride as coagulants. Desalin Water Treat. 2019;163:358–65 https://doi.org/10.5004/dwt.2019.24552.
4. Liu M, Liu X, Wang P, Zhang X. N-doped three-dimensional graphene aerogel with a high loading of Ag particles as an efficient catalyst and antibacterial agent. Colloids Surf A Physicochem Eng Asp. 2021;626:126886 https://doi.org/10.1016/j.colsurfa.2021.126886.
5. Helbling DE, VanBriesen JM. Free chlorine demand and cell survival of microbial suspensions. Water Res. 2007;41:4424–34 https://doi.org/10.1016/j.watres.2007.06.006.
6. Rangel JM, Lopez B, Mejia MA, Mendoza C, Luby S. A novel technology to improve drinking water quality: a microbiological evaluation of in-home flocculation and chlorination in rural Guatemala. J Water Health. 2003;1:15–22.
7. Aboubaraka AE, Aboelfetoh EF, Ebeid EZM. Coagulation effectiveness of graphene oxide for the removal of turbidity from raw surface water. Chemosphere. 2017;181:738–46 https://doi.org/10.1016/j.chemosphere.2017.04.137.
8. Wang J, Sui M, Yuan B, Li H, Lu H. Inactivation of two mycobacteria by free chlorine: effectiveness, influencing factors, and mechanisms. Sci Total Environ. 2019;648:271–84 https://doi.org/10.1016/j.scitotenv.2018.07.451.
9. Macauley JJ, Qiang Z, Adams CD, Surampalli R, Mormile MR. Disinfection of swine wastewater using chlorine, ultraviolet light and ozone. Water Res. 2006;40:2017–26 https://doi.org/10.1016/j.watres.2006.03.021.
10. Ren L, Chen J, Lu Q, Wang C, Han J, Huang K, Pan X, Wu H. Construction of high selectivity and antifouling nanofiltration membrane via incorporating macrocyclic molecules into active layer. J Memb Sci. 2020;597:117641 https://doi.org/10.1016/j.memsci.2019.117641.
11. Gomes JF, Lopes A, Gonçalves D, Luxo C, Gmurek M, Costa R, Quinta-Ferreira RM, Martins RC, Matos A. Biofiltration using C. fluminea for E.coli removal from water: comparison with ozonation and photocatalytic oxidation. Chemosphere. 208, 2018:674–81 https://doi.org/10.1016/j.chemosphere.2018.06.045.
12. Moradlou O, Rabiei Z, Delavari N. Antibacterial effects of carbon quantum dots@hematite nanostructures deposited on titanium against gram-positive and gram-negative bacteria. J Photochem Photobiol A Chem. 2019;379:144–9 https://doi.org/10.1016/j.jphotochem.2019.04.047.
13. Marković ZM, Kováčová M, Humpolíček P, Budimir MD, Vajďák J, Kubát P, Mičušík M, Švajdlenková H, Danko M, Capáková Z, Lehocký M, Todorović Marković BM, Špitalský Z. Antibacterial photodynamic activity of carbon quantum dots/polydimethylsiloxane nanocomposites against Staphylococcus aureus, Escherichia coli and Klebsiella pneumoniae. Photodiagn Photodyn Ther. 2019;26:342–9 https://doi.org/10.1016/j.pdpdt.2019.04.019.
14. Karunakaran C, Abiramasundari G, Gomathisankar P, Manikandan G, Anandi V. Cu-doped TiO2 nanoparticles for photocatalytic disinfection of bacteria under visible light. J Colloid Interface Sci. 2010;352:68–74 https://doi.org/10.1016/j.jcis.2010.08.012.
15. Luo Y, Gao B, Yue Q, Li R. Application of enteromorpha polysaccharides as coagulant aid in the simultaneous removal of CuO nanoparticles and Cu2+: effect of humic acid concentration. Chemosphere. 2018;204:492–500 https://doi.org/10.1016/j.chemosphere.2018.03.168.
16. Jafari AJ, Arfaeinia H, Ramavandi B, Kalantary RR, Esrafily A. Ozone-assisted photocatalytic degradation of gaseous toluene from waste air stream using silica-functionalized graphene oxide/ZnO coated on fiberglass: performance, intermediates, and mechanistic pathways. Air Qual Atmos Heal. 2019;12:1181–8 https://doi.org/10.1007/s11869-019-00732-6.
17. Wei F, Li J, Dong C, Bi Y, Han X. Plasmonic Ag decorated graphitic carbon nitride sheets with enhanced visible-light response for photocatalytic water disinfection and organic pollutant removal. Chemosphere. 2020;242:1–11 https://doi.org/10.1016/j.chemosphere.2019.125201.
18. Zhang J, An X, Li X, Liao X, Nie Y, Fan Z. Enhanced antibacterial properties of the bracket under natural light via decoration with ZnO/carbon quantum dots composite coating. Chem Phys Lett. 2018;706:702–7 https://doi.org/10.1016/j.cplett.2018.06.029.
19. Abbas MW, Soomro RA, Kalwar NH, Zahoor M, Avci A, Pehlivan E, Hallam KR, Willander M. Carbon quantum dot coated Fe3O4 hybrid composites for sensitive electrochemical detection of uric acid. Microchem J. 2019;146:517–24 https://doi.org/10.1016/j.microc.2019.01.034.
20. Li S, Liu J, Chen Z, Lu Y, Low SS, Zhu L, Cheng C, He Y, Chen Q, Su B, Liu Q. Electrogenerated chemiluminescence on smartphone with graphene quantum dots nanocomposites for Escherichia Coli detection. Sensors Actuators B Chem. 2019;297 https://doi.org/10.1016/j.snb.2019.126811.
21. Yadav P, Nishanthi ST, Purohit B, Shanavas A, Kailasam K. Metal free visible light photocatalytic carbon nitride quantum dots as efficient antibacterial agents: An insight study. Carbon N Y. 2019;152:587–97 https://doi.org/10.1016/j.carbon.2019.06.045.
22. Huang Y, Liang Y, Rao Y, Zhu D, Cao JJ, Shen Z, Ho W, Lee SC. Environment-friendly carbon quantum dots/ZnFe2O4 Photocatalysts: characterization, biocompatibility, and mechanisms for NO removal. Environ Sci Technol. 2017;51:2924–33 https://doi.org/10.1021/acs.est.6b04460.
23. Qu Y, Xu X, Huang R, Qi W, Su R, He Z. Enhanced photocatalytic degradation of antibiotics in water over functionalized N,S-doped carbon quantum dots embedded ZnO nanoflowers under sunlight irradiation. Chem Eng J. 2020;382 https://doi.org/10.1016/j.cej.2019.123016.
24. Jafari AJ, Kalantari RR, Kermani M, Firooz MH. ZnO nanoparticles photocatalytic activity toward atmospheric toluene under simulated sunlight. Res Chem Intermed. 2020;46:119–31 https://doi.org/10.1007/s11164-019-03938-6.
25. Chen P, Wang F, Chen ZF, Zhang Q, Su Y, Shen L, Yao K, Liu Y, Cai Z, Lv W, Liu G. Study on the photocatalytic mechanism and detoxicity of gemfibrozil by a sunlight-driven TiO2/carbon dots photocatalyst: the significant roles of reactive oxygen species. Appl Catal B Environ. 2017;204:250–9 https://doi.org/10.1016/j.apcatb.2016.11.040.
26. Zhao C, Wang X, Wu L, Wu W, Zheng Y, Lin L, Weng S, Lin X. Nitrogen-doped carbon quantum dots as an antimicrobial agent

against staphylococcus for the treatment of infected wounds. Colloids Surfaces B Biointerfaces. 2019;179:17–27 https://doi.org/10.1016/j.colsurfb.2019.03.042.
27. Moradi M, Kalantary RR, Esrafili A, Jafari AJ, Gholami M. Visible light photocatalytic inactivation of Escherichia coli by natural pyrite assisted by oxalate at neutral pH. J Mol Liq. 2017;248:880–9 https://doi.org/10.1016/j.molliq.2017.10.115.
28. Zeng X, Wang Z, Meng N, McCarthy DT, Deletic A, Pan JH, Zhang X. Highly dispersed TiO2 nanocrystals and carbon dots on reduced graphene oxide: ternary nanocomposites for accelerated photocatalytic water disinfection. Appl Catal B Environ. 2017;202:33–41 https://doi.org/10.1016/j.apcatb.2016.09.014.
29. Channei D, Inceesungvorn B, Wetchakun N, Phanichphant S. Kinetics study of photocatalytic activity of flame-made unloaded and Fe-loaded CeO2 nanoparticles. Int J Photoenergy. 2013;2013 https://doi.org/10.1155/2013/484831.
30. Bousslama W, Elhouichet H, Férid M. Enhanced photocatalytic activity of Fe doped ZnO nanocrystals under sunlight irradiation. Optik (Stuttg). 2017;134:88–98 https://doi.org/10.1016/j.ijleo.2017.01.025.
31. Hung W-H, Chien T-M, Lo A-Y, Tseng C-M, Li D. Spatially controllable plasmon enhanced water splitting photocurrent in au/TiO2-Fe2O3 cocatalyst system. RSC Adv. 2014;4:45710–4 https://doi.org/10.1039/c4ra05143b.
32. M. Mishra, D.M. Chun, α-Fe2O3 as a photocatalytic material: A review, Appl. Catal. A Gen. 498 (2015) 126–141. https://doi.org/10.1016/j.apcata.2015.03.023.
33. Li N, Zhang J, Tian Y, Zhao J, Zhang J, Zuo W. Precisely controlled fabrication of magnetic 3D γ-Fe2O3@ZnO core-shell photocatalyst with enhanced activity: ciprofloxacin degradation and mechanism insight. Chem Eng J. 2017;308:377–85 https://doi.org/10.1016/j.cej.2016.09.093.
34. Liu Y, Yu L, Hu Y, Guo C, Zhang F, Wen Lou X. A magnetically separable photocatalyst based on nest-like γ-Fe 2O 3/ZnO double-shelled hollow structures with enhanced photocatalytic activity. Nanoscale. 2012;4:183–7 https://doi.org/10.1039/c1nr11114k.
35. Chen Q, Chen L, Qi J, Tong Y, Lv Y, Xu C, Ni J, Liu W. Photocatalytic degradation of amoxicillin by carbon quantum dots modified K2Ti6O13 nanotubes: effect of light wavelength. Lett: Chinese Chem; 2019. https://doi.org/10.1016/j.cclet.2019.03.002
36. Chen T, Yin D, Zhang X, Zhao F, Kyu K, Deng L, Huang K, Li L, Liu J, Zhang Y. Fabrication of a novel carbon quantum dots-Modi fi ed 2D heterojunction for highly ef fi cient sunlight photocatalysis. J Alloys Compd. 2019;806:761–73 https://doi.org/10.1016/j.jallcom.2019.07.215.
37. Zhang M, Wang W, Cui Y, Chu X, Sun B, Zhou N, Shen J. Magnetofluorescent Fe3O4/carbon quantum dots coated single-walled carbon nanotubes as dual-modal targeted imaging and chemo/photodynamic/photothermal triple-modal therapeutic agents. Chem Eng J. 2018;338:526–38 https://doi.org/10.1016/j.cej.2018.01.081.
38. Kim SR, Jo WK. Boosted photocatalytic decomposition of nocuous organic gases over tricomposites of N-doped carbon quantum dots, ZnFe2O4, and BiOBr with different junctions. J Hazard Mater. 2019;380 https://doi.org/10.1016/j.jhazmat.2019.120866.
39. Muthulingam S, Lee IH, Uthirakumar P. Highly efficient degradation of dyes by carbon quantum dots/N-doped zinc oxide (CQD/N-ZnO) photocatalyst and its compatibility on three different commercial dyes under daylight. J Colloid Interface Sci. 2015;455:101–9 https://doi.org/10.1016/j.jcis.2015.05.046.
40. Gholami M, Mohammadi R, Arzanlou M, Akbari Dourbash F, Kouhsari E, Majidi G, Mohseni SM, Nazari S. In vitro antibacterial activity of poly (amidoamine)-G7 dendrimer. BMC Infect Dis. 2017;17:1–11 https://doi.org/10.1186/s12879-017-2513-7.
41. Taghavi K, Naghipour D, Mohagheghian A, Moslemzadeh M, Taghavi K, Moslemzadeh M, Pourkarim S, Ostovar F, Mahdavianpour M, Moslemzadeh M, Esrafili A, Bagheri S, Kermani M, Gholami M, Moslemzadeh M, Hahn HH. Adsorption of chromium(VI) from aqueous solution by Artist's bracket fungi. Water Sci Technol. 2017;158:207–15 https://doi.org/10.1080/01496395.2017.1299179.
42. Esrafili A, Bagheri S, Kermani M, Gholami M, Moslemzadeh M. Simultaneous adsorption of heavy metal ions (Cu2+ and Cd2+) from aqueous solutions by magnetic silica nanoparticles (Fe3O4@SiO2) modified using edta. Desalin Water Treat. 2019;158:207–15 https://doi.org/10.5004/dwt.2019.24274.
43. Naghipour D, Taghavi K, Moslemzadeh M. Removal of methylene blue from aqueous solution by Artist's bracket fungi: kinetic and equilibrium studies. Water Sci Technol. 2016;73:2832–40 https://doi.org/10.2166/wst.2016.147.
44. L. Li, C.G. Niu, H. Guo, J. Wang, M. Ruan, L. Zhang, C. Liang, H.Y. Liu, Y.Y. Yang, Efficient degradation of Levofloxacin with magnetically separable ZnFe2O4/NCDs/Ag2CO3 Z-scheme heterojunction photocatalyst: Vis-NIR light response ability and mechanism insight, Chem. Eng. J. 383 (2020). https://doi.org/10.1016/j.cej.2019.123192.
45. Y. Huang, D. Zhu, Q. Zhang, Y. Zhang, J. ji Cao, Z. Shen, W. Ho, S.C. Lee, Synthesis of a Bi2O2CO3/ZnFe2O4 heterojunction with enhanced photocatalytic activity for visible light irradiation-induced NO removal, Appl. Catal. B Environ. 234 (2018) 70–78. https://doi.org/10.1016/j.apcatb.2018.04.039.
46. Aghamali A, Khosravi M, Hamishehkar H, Modirshahla N, Behnajady MA. Preparation of novel high performance recoverable and natural sunlight-driven nanocomposite photocatalyst of Fe3O4/C/TiO2/N-CQDs. Mater Sci Semicond Process. 2018;87:142–54 https://doi.org/10.1016/j.mssp.2018.07.018.
47. Ahmadian-Fard-Fini S, Salavati-Niasari M, Ghanbari D. Hydrothermal green synthesis of magnetic Fe3O4-carbon dots by lemon and grape fruit extracts and as a photoluminescence sensor for detecting of E. coli bacteria, Spectrochim. Acta - part a Mol. Biomol. Spectrosc. 2018;203:481–93 https://doi.org/10.1016/j.saa.2018.06.021.
48. Mashkani M, Mehdinia A, Jabbari A, Bide Y, Nabid MR. Preconcentration and extraction of lead ions in vegetable and water samples by N-doped carbon quantum dot conjugated with Fe3O4 as a green and facial adsorbent. Food Chem. 2018;239:1019–26 https://doi.org/10.1016/j.foodchem.2017.07.042.
49. Chandra S, Chowdhuri AR, Mahto TK, Sahu SK. Nanostructured Fe3O4@Fe2O3/carbon dots heterojunction for efficient photocatalyst under visible light. J Nanosci Nanotechnol. 2017;17:1116–24 https://doi.org/10.1166/jnn.2017.12580.
50. Muthulingam S, Bin Bae K, Khan R, Lee IH, Uthirakumar P. Carbon quantum dots decorated N-doped ZnO: synthesis and enhanced photocatalytic activity on UV, visible and daylight sources with suppressed photocorrosion. J Environ Chem Eng. 2016;4:1148–55 https://doi.org/10.1016/j.jece.2015.06.029.
51. Medina-Ramírez IE, Arzate-Cardenas MA, Mojarro-Olmos A, Romo-López MA. Synthesis, characterization, toxicological and antibacterial activity evaluation of cu@ZnO nanocomposites. Ceram Int. 2019;45:17476–88 https://doi.org/10.1016/j.ceramint.2019.05.309.
52. Sen Chang J, Strunk J, Chong MN, Poh PE, Ocon JD. Multidimensional zinc oxide (ZnO) nanoarchitectures as efficient photocatalysts: what is the fundamental factor that determines photoactivity in ZnO? J Hazard Mater. 2020;381 https://doi.org/10.1016/j.jhazmat.2019.120958.
53. Moradlou O, Rabiei Z, Delavari N. Antibacterial effects of carbon quantum dots@hematite nanostructures deposited on titanium against gram-positive and gram-negative bacteria. J Photochem

Photobiol A Chem. 2019;379:144–9 https://doi.org/10.1016/j.jphotochem.2019.04.047.
54. Zhang XY, Liu JK, Wang JD, Yang XH. Mass production, enhanced visible light photocatalytic efficiency, and application of modified ZnO nanocrystals by carbon dots. Ind Eng Chem Res. 2015;54:1766–72 https://doi.org/10.1021/ie504444w.
55. Kuang W, Zhong Q, Ye X, Yan Y, Yang Y, Zhang J, Huang L, Tan S, Shi Q. Antibacterial Nanorods made of carbon quantum dots-ZnO under visible light irradiation. J Nanosci Nanotechnol. 2019;19:3982–90 https://doi.org/10.1166/jnn.2019.16320.
56. Wang Y, Ni P, Jiang S, Lu W, Li Z, Liu H, Lin J, Sun Y, Li Z. Highly sensitive fluorometric determination of oxytetracycline based on carbon dots and Fe3O4 MNPs. Sensors Actuators B Chem. 2018;254:1118–24 https://doi.org/10.1016/j.snb.2017.07.182.
57. S. Kourdali, A. Badis, A. Boucherit, K. Boudjema, A. Saiba, Electrochemical disinfection of bacterial contamination : E ff ectiveness and modeling study of E . coli inactivation by electro-Fenton , electro-peroxi- coagulation and electrocoagulation, J Environ Manag 226 (2018) 106–119. https://doi.org/10.1016/j.jenvman.2018.08.038.
58. He J, Zeng X, Lan S, Lo IMC. Reusable magnetic Ag/Fe, N-TiO2/Fe3O4@SiO2 composite for simultaneous photocatalytic disinfection of E. coli and degradation of bisphenol a in sewage under visible light. Chemosphere. 2019;217:869–78 https://doi.org/10.1016/j.chemosphere.2018.11.072.
59. Eskandarabadi SM, Mahmoudian M, Farah KR, Abdali A, Nozad E, Enayati M. Active intelligent packaging film based on ethylene vinyl acetate nanocomposite containing extracted anthocyanin, rosemary extract and ZnO/Fe-MMT nanoparticles. Food Packag Shelf Life. 2019;22:100389 https://doi.org/10.1016/j.fpsl.2019.100389.
60. Ganesan V, Hariram M, Vivekanandhan S, Muthuramkumar S. Periconium sp. (endophytic fungi) extract mediated sol-gel synthesis of ZnO nanoparticles for antimicrobial and antioxidant applications. Mater Sci Semicond Process. 2020;105:104739 https://doi.org/10.1016/j.mssp.2019.104739.
61. Mortazavi-Derazkola S, Salavati-Niasari M, Mazhari M-P, Khojasteh H, Hamadanian M, Bagheri S. Magnetically separable Fe3O4@SiO2@TiO2 nanostructures supported by neodymium(III): fabrication and enhanced photocatalytic activity for degradation of organic pollution. J Mater Sci Mater Electron. 2017;28:14271–81 https://doi.org/10.1007/s10854-017-7286-7.